

# 1      Climatology, seasonality and trends of oceanic coherent 2      eddies

3      **Josué Martínez-Moreno<sup>1</sup>, Andrew McC. Hogg<sup>1</sup>, and Matthew England<sup>2</sup>**

4      <sup>1</sup>Research School of Earth Science and ARC Center of Excellence for Climate Extremes, Australian  
5      National University, Canberra, Australia

6      <sup>2</sup>Climate Change Research Centre (CCRC), UNSW Australia, Sydney NSW, Australia

## 7      **Key Points:**

- 8      • Kinetic energy of coherent eddies contain around 50% of the surface ocean kinetic  
9      energy budget.
- 10     • Seasonal cycle of the number of coherent eddies and coherent eddy amplitude re-  
11     veal a 3-6 month lag to wind forcing
- 12     • Seasonal lag between the number of coherent eddies and eddy amplitude.
- 13     • The coherent eddy amplitude has increase at a rate of 3 cm per decade since 1993.

14      **Abstract**

15      Ocean eddies influence regional and global climate through mixing and transport  
 16      of heat and properties. One of the most recognizable and ubiquitous feature of oceanic  
 17      eddies are vortices with spatial scales of tens to hundreds of kilometers, frequently re-  
 18      ferred as “mesoscale eddies” or “coherent eddies”. Coherent eddies are known to trans-  
 19      port properties across the ocean and to locally affect near-surface wind, cloud proper-  
 20      ties and rainfall patterns. Although coherent eddies are ubiquitous, yet their climatol-  
 21      ogy, seasonality and long-term temporal evolution remains poorly understood. Thus, we  
 22      examine the kinetic energy contained by coherent eddies and we present the annual, in-  
 23      terannual, and long-term changes of automatically identified coherent eddies from satel-  
 24      lite observations from 1993 to 2018. Around 50% of the kinetic energy contained by ocean  
 25      eddies corresponds to coherent eddies. Additionally, a strong hemispherical seasonal cy-  
 26      cle is observed, with a 3–6 months lag between the wind forcing and the response of the  
 27      coherent eddy field. Furthermore, the seasonality of the number of coherent eddies and  
 28      their amplitude reveals that the number of coherent eddies responds faster to the forc-  
 29      ing (~3 months), then the coherent eddy amplitude (which is lagged by ~6 months). Our  
 30      analysis highlights the relative importance of the coherent eddy field in the ocean ki-  
 31      netic energy budget, implies a strong response of the eddy number and eddy amplitude  
 32      to forcing at different time-scales, and showcases the seasonality, and multidecadal trends  
 33      of coherent eddy properties.

34      **Plain language summary**

35      **1 Introduction**

36      Mesoscale ocean variability with spatial scales of tens to hundreds of kilometers is  
 37      comprised of processes such as vortices, waves, and jets (Ferrari & Wunsch, 2009; Fu et  
 38      al., 2010). These mesoscale processes are highly energetic, and they play a crucial role  
 39      in the transport of heat, salt, momentum, and other tracers through the ocean (Wun-  
 40      sch & Ferrari, 2004; Wyrtki et al., 1976; Gill et al., 1974). Possibly, the most recogniz-  
 41      able and abundant process observed from satellites is mesoscale vortices. Although mesoscale  
 42      vortices are commonly referred to in literature as “mesoscale eddies”, this term is also  
 43      often used to describe the total mesoscale ocean variability (the time-varying component  
 44      of the mesoscale flow), thus, here we will refer to mesoscale vortices as *coherent eddies*.

45 Coherent eddies are quasi-circular currents. According to their rotational direction,  
46 the sea surface height anomaly within a coherent eddy can have a negative or positive  
47 sea surface height anomaly (cold-core and warm-core coherent eddies, respectively). This  
48 characteristic sea surface height signature of coherent eddies has been utilized to auto-  
49 matically identify and track coherent eddies from satellite altimetry (Cui et al., 2020;  
50 Martínez-Moreno et al., 2019; Ashkezari et al., 2016; Faghmous et al., 2015; Chelton et  
51 al., 2007). Automated identification algorithms of coherent eddies have shown their ubiq-  
52 uituity in the oceans, with a predominant influence at hotspots of eddy activity such as bound-  
53 ary currents and the Antarctic Circumpolar Current. In these regions, Chelton et al. (2011)  
54 estimated that coherent eddies contribute around 40–50% of the mesoscale kinetic en-  
55 ergy (Chelton et al., 2011) and thus a significant fraction of the total kinetic energy (Fer-  
56 rari & Wunsch, 2009). Although this unique estimate showcases the importance of the  
57 mesoscale coherent eddy field, the energy contained by coherent eddies was estimated  
58 by extracting the geostrophic velocities within the detected coherent eddies, thus it is  
59 possible it may contain energy from other processes. Coherent eddies are not only abun-  
60 dant and may have a large proportion of the surface kinetic energy budget, but they are  
61 also essential to ocean dynamics as concluded by many previous studies (Patel et al., 2020;  
62 Schubert et al., 2019; Pilo et al., 2015; Frenger et al., 2015, 2013; Beron-Vera et al., 2013;  
63 Siegel et al., 2011; Hogg & Blundell, 2006).

64 There is broad consensus that mesoscale eddy kinetic energy has a pronounced sea-  
65 sonal variability (Uchida et al., 2017; Kang & Curchitser, 2017; Qiu & Chen, 2004; Qiu,  
66 1999). Several hypotheses have been proposed to explain this seasonality including: sea-  
67 sonal variations of atmospheric forcing (Sasaki et al., 2014), seasonality of the mixed layer  
68 depth (Qiu et al., 2014; Callies et al., 2015), seasonality of the intensity of barotropic in-  
69 stability (Qiu & Chen, 2004), the variability of the baroclinic instability due to the sea-  
70 sonality of the vertical shear (Qiu, 1999), and a seasonal lag of the inverse energy cas-  
71 cade (energy is transported between scales from small to large; Arbic et al., 2013) in com-  
72 bination with the presence of a front in the mixed layer, which can lead to a seasonal  
73 cycle of the baroclinic instability (Qiu et al., 2014). On one hand, processes such as barotropic  
74 and baroclinic instabilities control the seasonality of coherent eddies in the ocean. On  
75 the other hand, recent studies using observations and eddy-permitting climate models  
76 suggest several long-term adjustments of the global ocean capable of long-term changes  
77 in the coherent eddy field. Such readjustments include a multidecadal increase in the ocean

78 stratification resulted from temperature and salinity changes (Li et al., 2020), a horizontal  
 79 readjustment of the sea surface temperature gradients (Ruela et al., 2020; Bouali et  
 80 al., 2017; Cane et al., 1997), and an intensification of the kinetic energy, eddy kinetic en-  
 81 ergy, and mesoscale eddy kinetic energy over the last 3 decades as a consequence of an  
 82 increase in wind forcing (Hu et al., 2020; Wunsch, 2020; Martínez-Moreno et al., 2021).  
 83 All these seasonal factors and long-term readjustments directly influence the annual and  
 84 decadal response of the coherent eddy field, however, the seasonality of the coherent com-  
 85 ponent of the eddy kinetic energy, as well as the seasonal cycle and trends of the coher-  
 86 ent eddy statistics remain unknown.

87 Here we present a new global climatology of the coherent eddy kinetic energy by  
 88 reconstructing the coherent eddy signature from satellite observations. Our climatology  
 89 documents the seasonal cycle of the coherent eddy kinetic energy, and seasonal cycle and  
 90 long-term trends of the coherent eddy properties over the satellite record. Moreover, we  
 91 conduct more detail analysis in regions where coherent eddies dominate the eddy kinetic  
 92 energy field. This paper is structured as follows: the data sources and methodology are  
 93 described in section 2. Then, we present the climatology, energy ratios, and global sea-  
 94 sonality of the coherent eddy kinetic energy in subsection 3. Subsection 4 presents the  
 95 global climatology and seasonality of coherent eddy properties, followed by the seasonal  
 96 cycle and coherent eddy property time-series in regions dominated by coherent eddies  
 97 (subsection 6.1). We then focus our attention on the long-term changes of the coherent  
 98 eddy properties (section 5). Finally, section 7 summarizes the main results and discusses  
 99 the implications of this study.

## 100 2 Methods

### 101 2.1 Data

102 We use daily sea surface height (SSH) data are available by the Copernicus Ma-  
 103 rine Environment Monitoring Service in near real time (CMEMS, 2017). This gridded  
 104 product contains the sea surface height and geostrophic velocities with daily  $0.25^{\circ}$  res-  
 105 olution from January 1993 to 2019. The daily geostrophic velocities allowed us to com-  
 106 pute the kinetic energy (KE) and eddy kinetic energy (EKE) over the satellite record.

107        The main source of EKE is the time-varying wind (Ferrari & Wunsch, 2009), thus  
 108        we computed the seasonal cycle of the wind magnitude from the JRA55 reanalysis (Tsu-  
 109        jino et al., 2018) using wind velocities at 10m above the ocean's surface.

110        Over the same record, coherent eddy statistics are gridded in a  $1^{\circ}$  resolution the  
 111        identified mesoscale coherent eddies datasets released by Chelton & Schlax (2013) and  
 112        Martínez-Moreno et al. (2019).

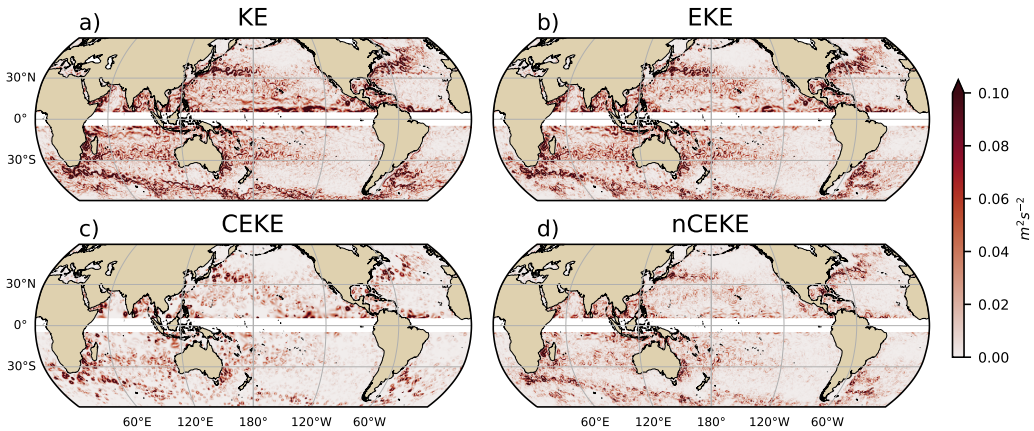
113        Although both dataset are produced via automated eddy identification algorithms  
 114        using closed contours of SSH, these datasets have significant differences in the criteria  
 115        they use to identify and record coherent eddies statistics. The major difference include:  
 116        (i) Martinez's algorithm requires an good adjustment between a 2D Gaussian and the  
 117        SSH anomaly (SSH<sub>a</sub>) surface within the identify closed contour, while Chelton's only uses  
 118        the outer-most closed contour of SSH; (ii) Martinez's dataset reports the maximum SSH<sub>a</sub>  
 119        within the identified coherent eddy, while Chelton's algorithm reports the maximum SSH  
 120        value minus the discrete level in which the coherent eddy was identified; Martinez's dataset  
 121        includes all detected coherent eddies, while Chelton's dataset excludes (iii) coherent ed-  
 122        dies with lifetimes shorter than four weeks and (iv) coherent eddy amplitudes smaller than  
 123        1cm. Moreover, Martinez's algorithm allows the reconstruction of the coherent eddy field  
 124        under the assumption that coherent eddies have a 2D Gaussian imprint in the sea sur-  
 125        face height. These Gaussian anomalies then allow us to estimate the coherent geostrophic  
 126        eddy velocities and thus the kinetic energy contained only by coherent eddies.

127        In this study, we analyze the climatology, seasonal cycles and trends of the eddy  
 128        statistics between 1993 and 2019, moreover, we exclude the equatorial region ( $10^{\circ}\text{S}$  -  $10^{\circ}\text{N}$   
 129        ) and poleward of  $60^{\circ}$ . Seasonal climatologies are calculated by monthly averages, while  
 130        hemispherical time-series are filtered with a running average of 90 days. Trends

131        **Define mean abs eddy amplitude and eddy count.**

## 132        2.2 Kinetic Energy decomposition

133        Kinetic energy is commonly divided into the mean and time-varying components  
 134        through a Reynolds decomposition. At a given time, the velocity field  $\mathbf{u} = (u, v)$  is split  
 135        into the time mean ( $\bar{\mathbf{u}}$ ) and time varying components ( $\mathbf{u}'$ ). Additionally, we further de-



144 **Figure 1.** Snapshot of surface kinetic energy ( $\overline{KE}$ ), surface eddy kinetic energy ( $\overline{EKE}$ ),  
 145 surface coherent eddy kinetic energy ( $\overline{CEKE}$ ), and surface non-coherent eddy kinetic energy  
 146 ( $\overline{nCEKE}$ ) for the 1st of January 2017.

136 compose the eddy kinetic energy into the eddy kinetic energy contained by coherent fea-  
 137 tures ( $\mathbf{u}'_e$ ) and non-coherent ( $\mathbf{u}'_n$ ). Therefore the KE equation can be written as:

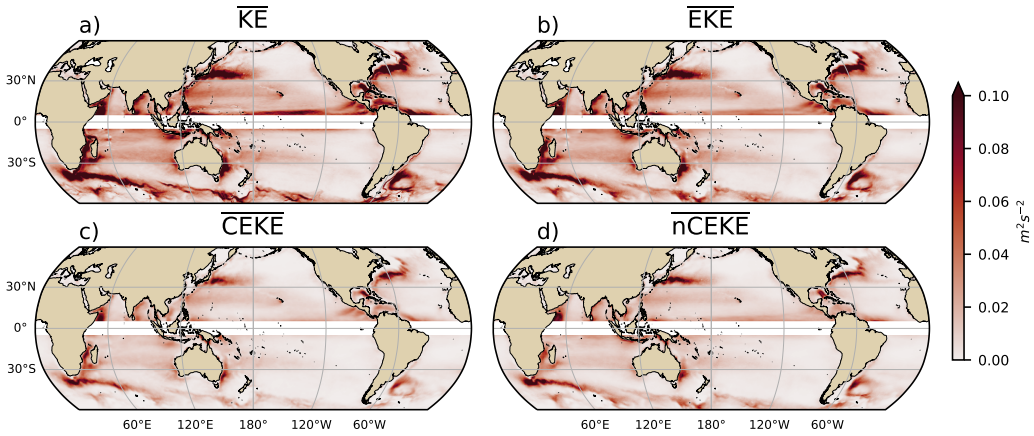
$$KE = \underbrace{\bar{u}^2 + \bar{v}^2}_{MKE} + \underbrace{u'^2_e + v'^2_e}_{CEKE} + \underbrace{u'^2_n + v'^2_n}_{nCEKE} + \mathcal{O}_c^2 + \mathcal{O}^2 \quad (1)$$

138 Due to the properties of this decomposition, the second order term  $\mathcal{O}^2$  is zero when av-  
 139 eraged over the same period as  $\bar{\mathbf{u}}$ . However,  $\mathcal{O}_c^2$  is only negligible when averaged in time  
 140 and space. For more information about the decomposition of the field into coherent fea-  
 141 tures and non-coherent features refer to Martínez-Moreno et al. (2019). A global snap-  
 142 shot of each component of kinetic energy decomposition is shown in figure 1, where the  
 143 imprint of the coherent eddies corresponds to rings of kinetic energy.

147 we divide the Southern Ocean up into the three sectors similar to those used by  
 148 MH06 (Indian Ocean: 40E–150E, 57S–44S; Pacific Ocean: 150E–288E, 62S–48S; and At-  
 149 lantic Ocean: 325E–10E, 56S–46S). The regional analysis indicates that the long-term  
 150 trend in Southern Ocean wind stress is dominated by changes in the Pacific sector.

### 151 3 Global Coherent Eddy Energetics

152 **Figure 2**



158 **Figure 2.** Climatology of surface kinetic energy ( $\overline{KE}$ ), surface eddy kinetic energy ( $\overline{EKE}$ ),  
 159 surface coherent eddy kinetic energy ( $\overline{CEKE}$ ), and surface non-coherent eddy kinetic energy  
 160 ( $\overline{nCEKE}$ ) between 1993-2018.

- 153 • All KE components have large energy contents in the boundary currents and antarc-  
 154 tic circumpolar current.
- 155 • In many cases is the same, but there actually some differences There are several  
 156 regions where the coherent component is larger than the non-coherent, we will in-  
 157 vestigate these in more detail in section XX.

161 **Figure 3**

- 162 •  $\overline{EKE}$  is responsible of almost all the  $\overline{KE}$  across the ocean, except for regions with  
 163 persistent currents over time, such as the mean boundary current locations, equa-  
 164 torial pacific currents and regions in the Antarctic Circumpolar current, where the  
 165 EKE explains around 40% of the  $\overline{KE}$
- 166 • This estimate is consistent with that of Chelton.
- 167 •  $\overline{EKE}$  Explains 80% of  $\overline{KE}$ , while  $\overline{CEKE}$  is 45% of  $\overline{EKE}$  and  $\overline{nCEKE}$  is 60% of  
 168  $\overline{EKE}$
- 169 •  $\overline{CEKE}$  is large equatorwards from the Kuroshio current and Agulhas current.
- 170 • Areas with the largest coherent contribution are located in the South of Australia  
 171  $\overline{CEKE}$  and South Atlantic
- 172 •

- $\overline{nCEKE}$  has a large amount of energy at high latitudes, this could be a consequence of the satellites not resolving the mesoscale coherent eddies.
- Global averages of the ratios show  $\overline{EKE}$  explains around 78% of the ocean  $MKE$  field, while coherent eddies and non coherent eddy features contain 49% and 59% per decade. Note this values don't add to 1 as there are cross terms that contain around XX% of the total energy.

### 187      *3.0.1 Seasonality*

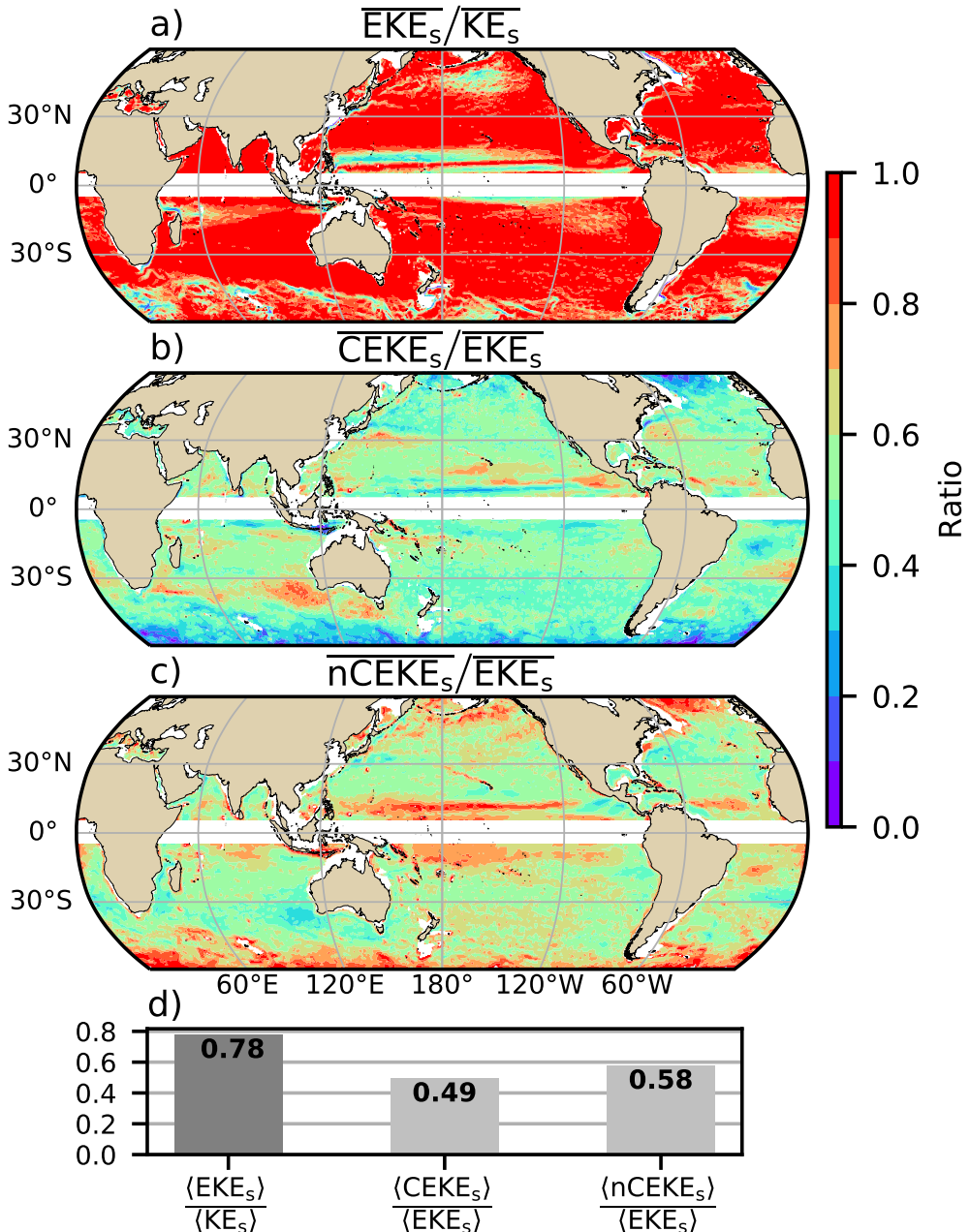
#### 188      **Figure 4**

- The hemisphere seasonality show the EKE and CEKE peak in summer.
- Response of the EKE and CEKE show a seasonal lag of  $\sim$ 6 months to the forcing of the Winds. Make sure to note the maximum over the hemisphere, locally, the winds may peak in different months.
- Methods, explain more about winds or here.
- The coherent eddy field show a large interannual variability.
- In the Southern Ocean we observe a concentric growth as time passes, which support the increasing trends in the Southern Ocean observed by (Hogg et al., 2015; Martínez-Moreno et al., 2019, 2021)
- Point that in the northern hemisphere in winter the CEKE appears to be decreasing.

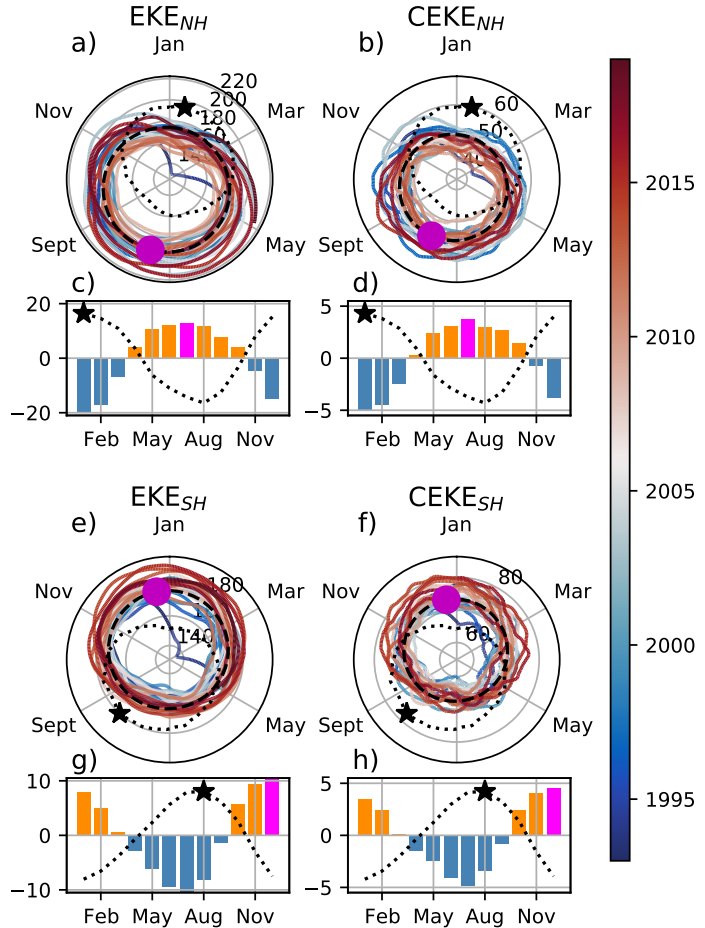
## 206      **4 Global Coherent Eddy Statistics**

#### 207      **Figure 5**

- A comparison with previous identified numbers show a consistent pattern in the eddy count. The difference in the magnitude could be a consequence of Chelton et al. (2007) filtering the coherent eddies with lifespans longer than 16 weeks.
- Both datasets show a large number of eddies in the East North Pacific, East North Atlantic, as well as the East South Pacific, East South Atlantic and East Indian Ocean.
- While the number of eddies detected in the tropics is quite small.



179 **Figure 3.** Ratios of the kinetic energy components. a) Map of the proportion of mean eddy  
 180 kinetic energy ( $EKE_s$ ) versus mean kinetic energy ( $\overline{KE}$ ); b) Map of the percentage of mean co-  
 181 herent eddy kinetic energy ( $\overline{CEKE}_s$ ) versus mean eddy kinetic energy ( $\overline{EKE}_s$ ); c) Map of the  
 182 percentage of mean non-coherent eddy kinetic energy ( $\overline{nCEKE}_s$ ) versus mean eddy kinetic energy  
 183 ( $\overline{EKE}_s$ ); d) Global averaged percentage of mean eddy kinetic energy ( $\langle \overline{EKE} \rangle$ ) versus the global  
 184 mean kinetic energy ( $\langle \overline{KE} \rangle$ ), and percentage of mean coherent eddy kinetic energy ( $\langle \overline{CEKE} \rangle$ )  
 185 and mean non coherent eddy kinetic energy ( $\langle \overline{nCEKE} \rangle$ ) versus global mean eddy kinetic energy  
 186 ( $\langle \overline{EKE} \rangle$ ).



200 **Figure 4.** Hemispherical seasonality of eddy kinetic energy (EKE), coherent eddy kinetic en-  
 201 ergy (CEKE). Panels a, and b show the northern hemisphere seasonal cycle, while panels c, and  
 202 d correspond to the southern hemisphere. Dashed lines correspond to the seasonal cycle of the  
 203 fields and dotted lines show the seasonal cycle of the wind magnitude smoothed over 120 days  
 204 (moving average). The green and magenta stars show the maximum of the seasonal cycle for the  
 205 kinetic energy components and the wind magnitude, respectively. The line colors show the year.

- Furthermore, there are hotspots of numbers of eddies in other regions of the ocean, such as boundary currents and the Antarctic Circumpolar Current.
- An interesting feature shown in both datasets is a predominant patchiness where the count of the eddies is much larger. These puzzling pattern remains unknown. Although it looks like a propagation pattern, it could be that eddies persist for longer in those areas.
- The eddy amplitude as expected is maximum at the boundary currents and hotspots in the southern ocean.
- Interior of the gyres we can observe that there is an important amplitude of the coherent eddy field.
- Preferred eddy amplitude sign in boundary currents; positive amplitude polewards to the boundary current mean location, and negative amplitude equatorwards. This is consistent with the shed of coherent eddies from the boundary currents.
- There regions with large CEKE ratio show also a large coherent eddy amplitude.
- Absolute eddy amplitude has the similar signature as CEKE.

#### 4.0.1 Seasonality

##### Figure 6

- Seasonality of the number of eddies in the Northern Hemisphere peaks on May, while the Southern Hemisphere peaks on October.
- The seasonality of the amplitude of the eddies is consistent with those of the Coherent eddy kinetic energy.
- Interestingly, there is a 3 month lag between the winds and the seasonality of the number of eddies, while the eddy amplitude responds approximately 6 months after the maximum winds.
- Note that both coherent eddy amplitudes seem to peak around the same time.
- If we look closely, the growing-shrinking concentric circles correspond to an increasing-decreasing trend. These are particularly obvious as a decrease in the eddy number in the Southern Hemisphere, and an increase in the eddy amplitude.

##### Figure 6

- a

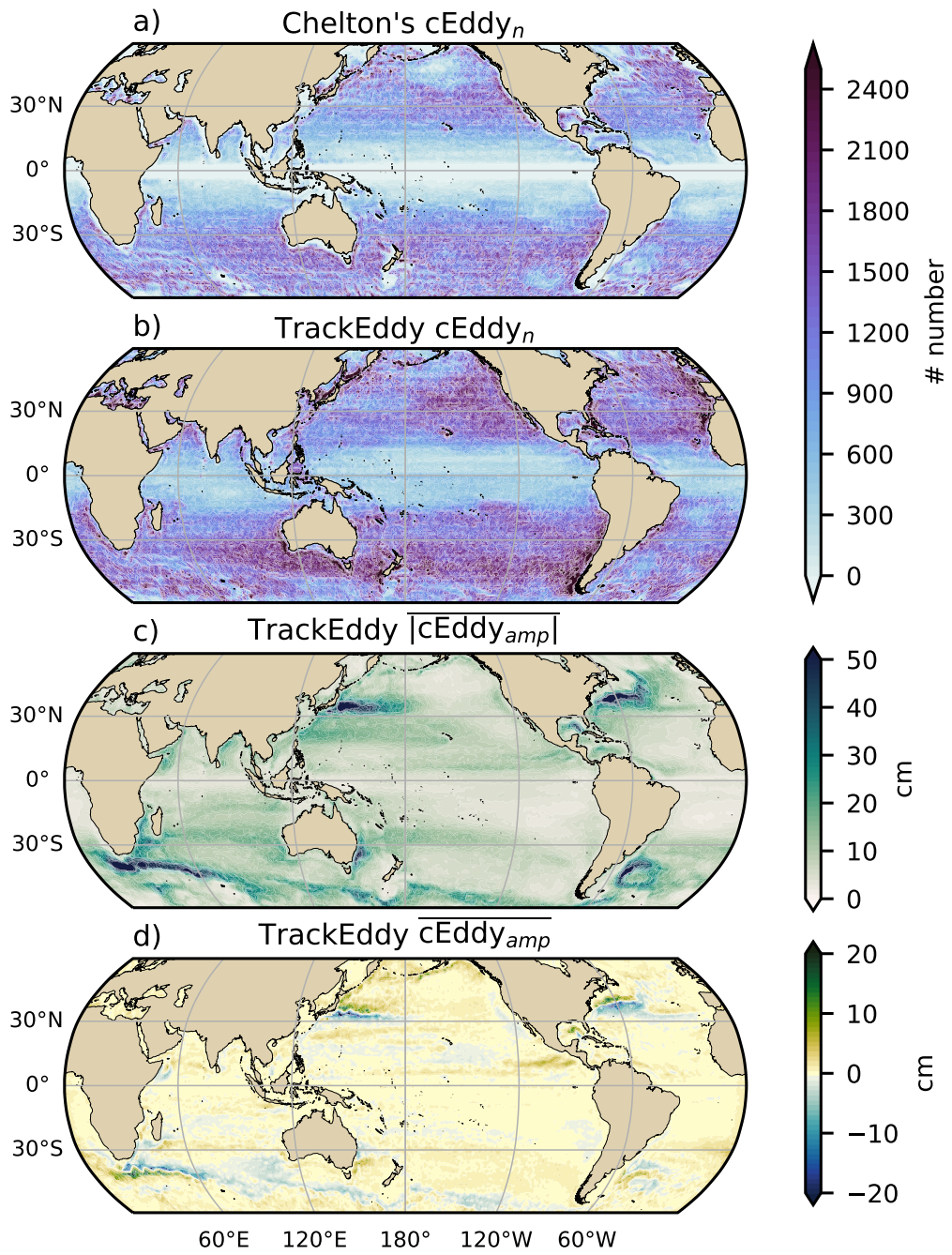
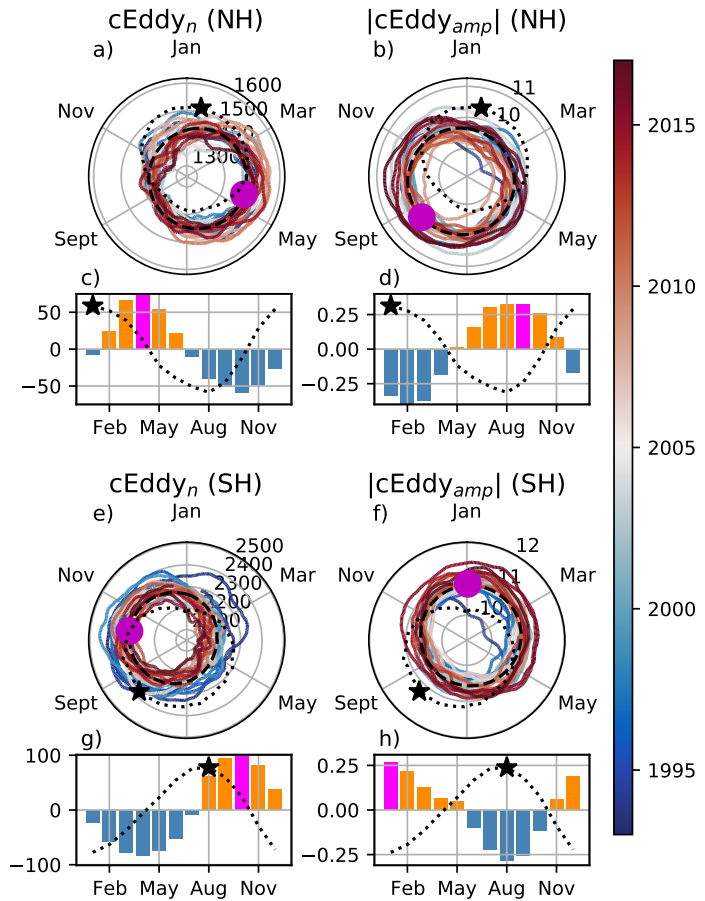


**Figure 5.** Climatology of the coherent eddy statistics. a) Climatology of the number of coherent eddies ( $cEddy_n$ ) identified by Chelton et al. (2007); b) Climatology of the number of coherent eddies ( $cEddy_n$ ) identified by Martínez-Moreno et al. (2019); c) Climatology of the mean absolute coherent eddy amplitude ( $cEddy_{amp}$ ). d) Climatology of the mean coherent eddy amplitude ( $cEddy_{amp}$ ).



248 **Figure 6.** Hemispherical seasonality of the coherent eddy statistics; a,e) seasonal cycle of the  
 249 number of coherent eddies ( $cEddy_n$ ); b,f) seasonal cycle of the mean coherent eddy amplitude  
 250 ( $cEddy_{amp}$ ); c,g) seasonal cycle of the warm core coherent eddies amplitude (positive  $cEddy_{amp}$ );  
 251 d,h) seasonal cycle of the cold core coherent eddies amplitude (negative  $cEddy_{amp}$ ). Panels a,b  
 252 and c show the northern hemisphere seasonal cycle, while panels d,e, and f correspond to the  
 253 southern hemisphere. Dashed lines correspond to the seasonal cycle of the fields and dotted lines  
 254 show the seasonal cycle of the wind magnitude smoothed over 120 days (moving average). The  
 255 green and magenta stars show the maximum of the seasonal cycle for each field and the wind  
 256 magnitude, respectively. The line colors show the year.

268 **5 Trends**269 **Figure 13**

- 270 • The number and amplitude of coherent eddies from two eddy tracking algorithms  
271 show consistent trend patterns.
- 272 • In particular, we observe a decrease in the number of eddies in the southern ocean,  
273 as well as sectors in the North Atlantic and North Pacific.
- 274 • Meanwhile the amplitude seems to be increasing in those same regions.
- 275 • Some of these regions have undergone a readjustment to stronger winds, thus the  
276 observed trends in the eddy amplitude suggests an intensification of the coherent  
277 eddy field to an increase in the forcing.
- 278 • This increase is consistent with Martínez-Moreno et al. (2021)

285 **6 Regional**286 **6.1 Boundary Currents**287 **Figure 10**

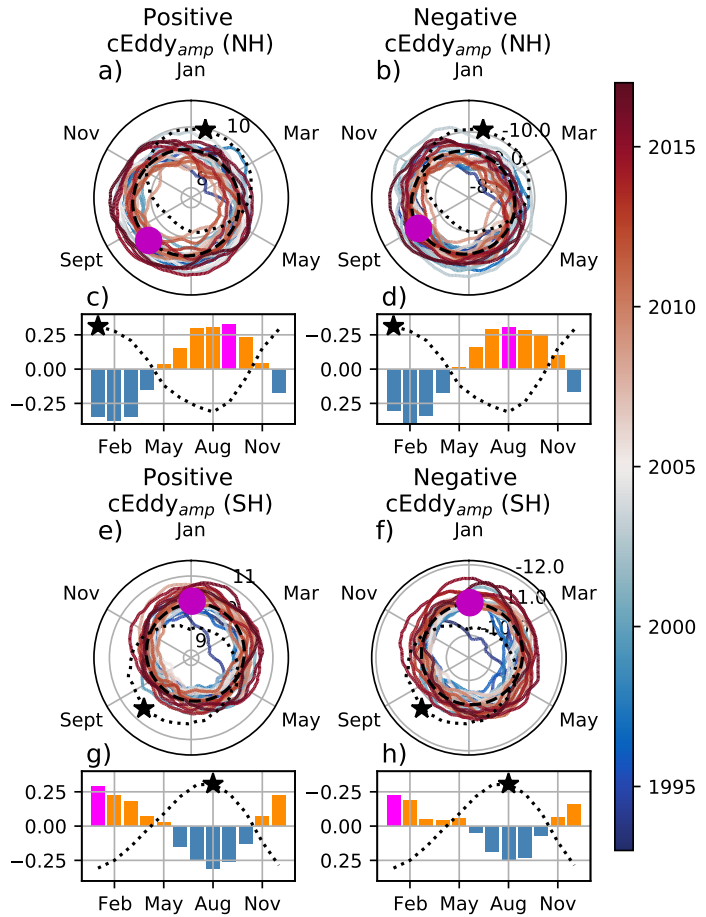
- 288 • Described similar to figure 7, 8, and 9
- 289 • Note that boundary currents have a consistent seasonal cycle in the positive and  
290 negative eddy amplitude.
- 291 • As expected, the seasonal cycle is opposite to BC in the northern hemisphere.

293 **Figure 11**

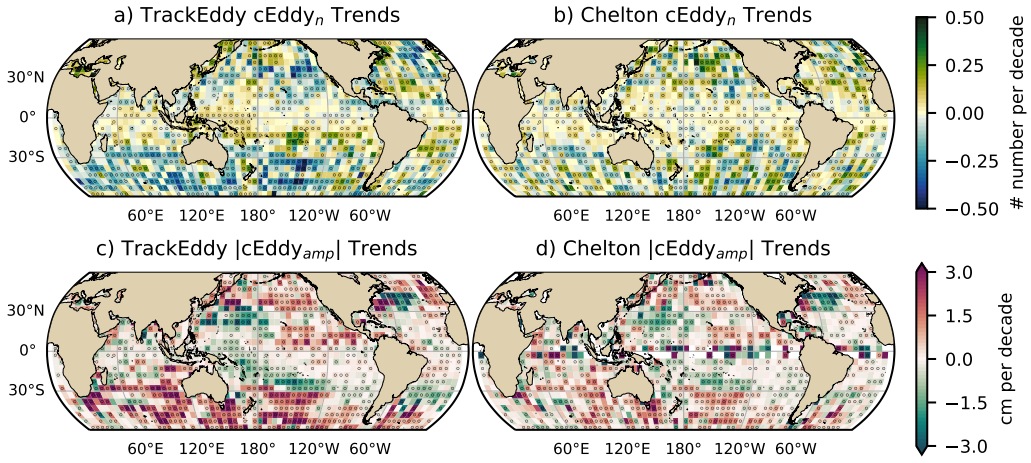
- 294 • Described similar to figure 7, 8, and 9
- 295 • Note that boundary currents have a consistent seasonal cycle in the positive and  
296 negative eddy amplitude.

298 **Figure 12**

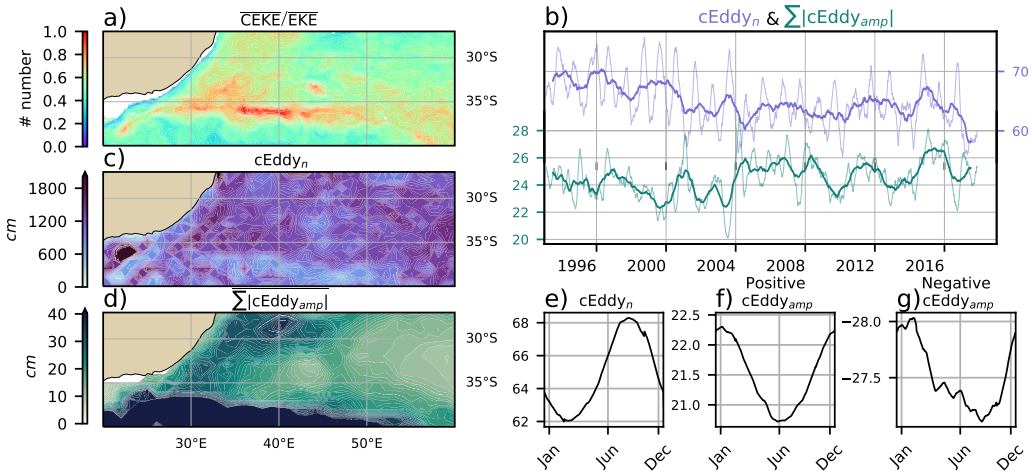
- 299 • Described similar to figure 7, 8, and 9
- 300 • Note that boundary currents have a consistent seasonal cycle in the positive and  
301 negative eddy amplitude.
- 302 • Delete Fig 11 or 12, they are really similar. What do you think?



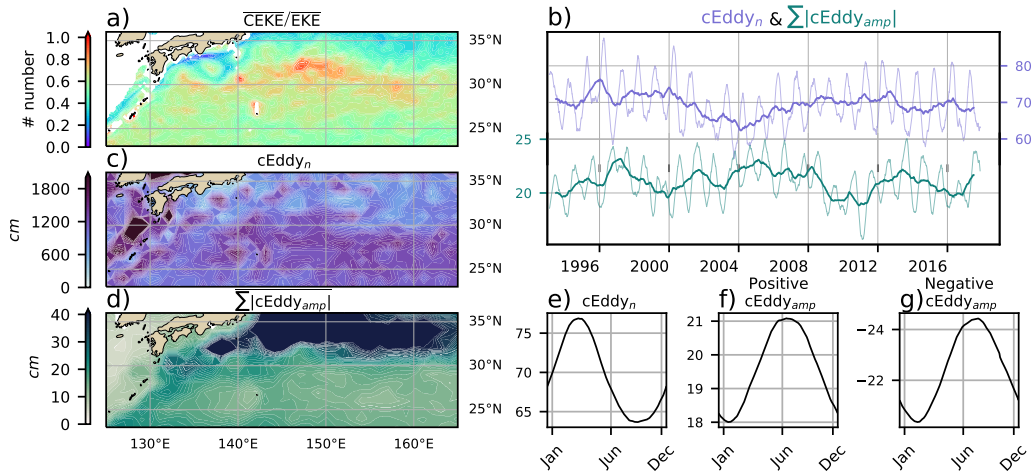
259 **Figure 7.** Hemispherical seasonality of the coherent eddy statistics; a,e) seasonal cycle of the  
 260 number of coherent eddies ( $cEddy_n$ ); b,f) seasonal cycle of the mean coherent eddy amplitude  
 261 ( $cEddy_{amp}$ ); c,g) seasonal cycle of the warm core coherent eddies amplitude (positive  $cEddy_{amp}$ );  
 262 d,h) seasonal cycle of the cold core coherent eddies amplitude (negative  $cEddy_{amp}$ ). Panels a,b  
 263 and c show the northern hemisphere seasonal cycle, while panels d,e, and f correspond to the  
 264 southern hemisphere. Dashed lines correspond to the seasonal cycle of the fields and dotted lines  
 265 show the seasonal cycle of the wind magnitude smoothed over 120 days (moving average). The  
 266 green and magenta stars show the maximum of the seasonal cycle for each field and the wind  
 267 magnitude, respectively. The line colors show the year.



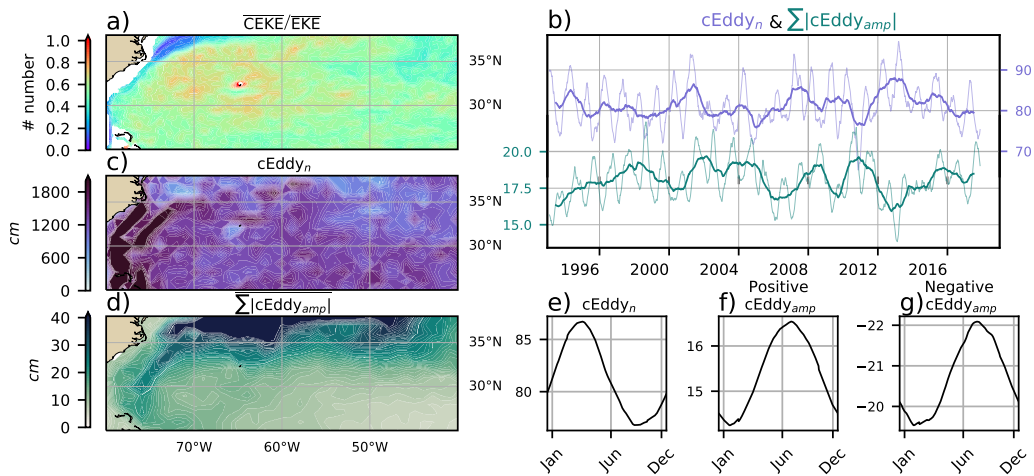
279 **Figure 8.** Trends of coherent eddy statistics. a) and b) Trends of the number of identified  
 280 coherent eddies from satellite observations identified using TrackEddy, and those reported in  
 281 Chelton's dataset. c) and e) Trends of the mean absolute value of identified coherent eddies am-  
 282 plitude from satellite observations identified using TrackEddy, and those reported in Chelton's  
 283 dataset. Gray stippling shows regions that are statistically significant above the 95% confidence  
 284 level.



292 **Figure 9.** Same as Figure 12 but for the Agulhas Current.



297

**Figure 10.** Same as Figure 12 but for the Kuroshio Current.

303

**Figure 11.** Move to supplementary Same as Figure 12 but for the Gulf Stream.

304 **6.2 Eastern currents**305 **Figure 7**

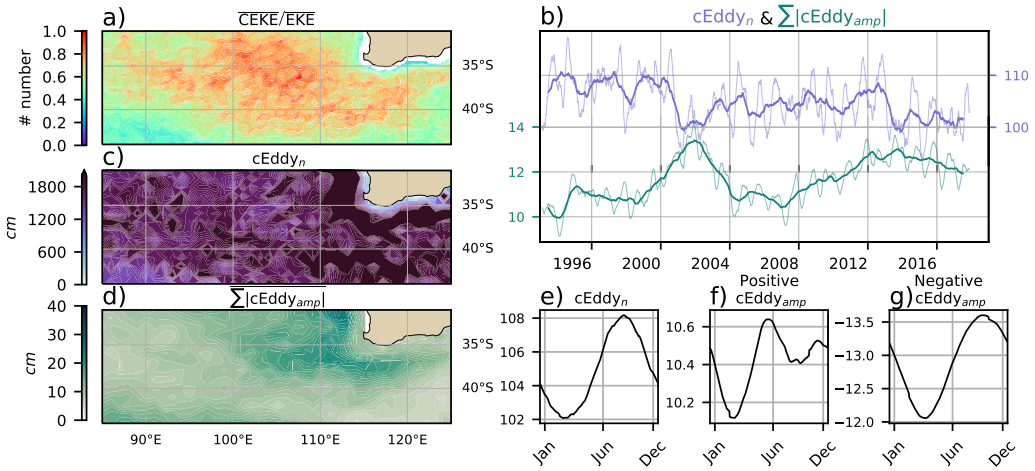
- 306 • South of the Leeuwin Current there is an important dominance fo the coherent  
307 eddy field, where it explains around 80% of the eddy kinetic energy.
- 308 • Although this region does not have a large EKE, we can observe a considerable  
309 amount of eddies across the region, but more importantly the coherent eddy am-  
310 plitude is particularly large in those regions with coherent eddy dominance.
- 311 • The solid lines show an decrease in the number of eddies, but an increase in the  
312 eddy amplitude.
- 313 • Moreover, the coherent eddy number peaks in August.
- 314 • Meanwhile coherent eddies with the positive amplitude have a smaller amplitude  
315 than the negative, furthermore, the positive eddies peak in Jun and show a inter-  
316 annual modulation, while the negative eddies peak in October.
- 317 • Research regional dynamics (Add here why we may expect this response.)

325 **Figure 9**

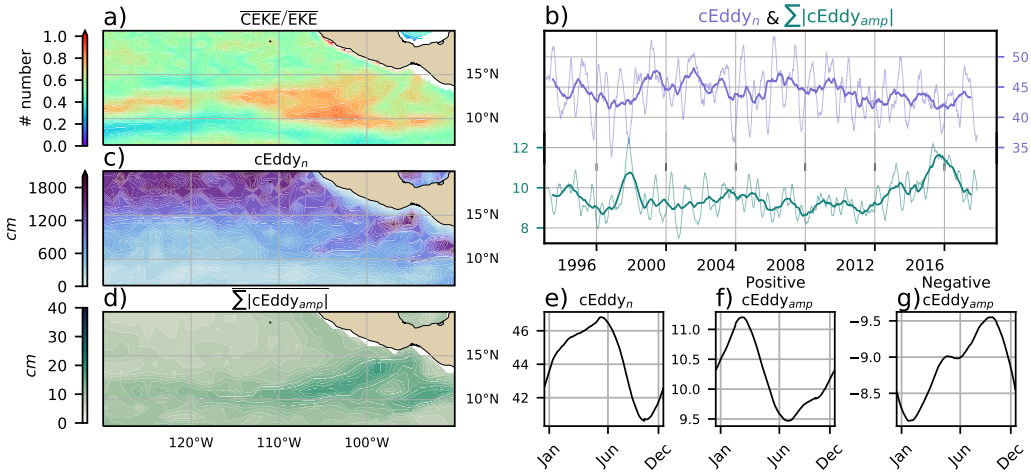
- 326 • Here we observe that the number of eddies and eddy amplitude are large in the  
327 area where the coherent eddies dominate the eddy field.
- 328 • Dynamically, in this region eddies are generated due to Rossby wave propagation  
329 along the coast that becomes unstable and sheds eddies at the Tehuantepec Gulf.
- 330 • The seasonal cycle shows a peak in Jun, while the positive amplitude is observed  
331 in March and the negative amplitude maximum occurs in September.
- 332 • Research regional dynamics (Add here why we may expect this response.)

334 **7 Summary and Conclusions**335 **Acknowledgments**

336 Chelton & Schlax (2013) dataset was produced by SSALTO/DUACS and distributed by  
337 AVISO+ (<https://www.aviso.altimetry.fr/>) with support from CNES, developed  
338 and validated in collaboration with E.Mason at IMEDEA.



318 **Figure 12.** Climatology of the eddy field and coherent eddy field at the Leeuwin Current. a)  
 319 Ratio of mean coherent eddy kinetic energy ( $\overline{\text{CEKE}}$ ) versus mean eddy kinetic energy ( $\overline{\text{EKE}}$ ); b)  
 320 Thick lines show the running average over 2 years and thin lines show the running average over  
 321 90 days of the coherent eddy number sum and the average absolute coherent eddy amplitude; c)  
 322 Map of the number of eddies; d) Map of the average absolute coherent eddy amplitude; e) Sea-  
 323 sonal cycle of the number of eddies f) Seasonal cycle of the positive coherent eddy amplitude. g)  
 324 Seasonal cycle of the negative coherent eddy amplitude.



333 **Figure 13.** Same as Figure 12 but for the East Tropical Pacific.

339 **References**

- 340 Arbic, B. K., Polzin, K. L., Scott, R. B., Richman, J. G., & Shriver, J. F. (2013).  
 341 On Eddy Viscosity, Energy Cascades, and the Horizontal Resolution of Gridded  
 342 Satellite Altimeter Products\*. *Journal of Physical Oceanography*, 43(2), 283–300.  
 343 doi: 10.1175/jpo-d-11-0240.1
- 344 Ashkezari, M. D., Hill, C. N., Follett, C. N., Forget, G., & Follows, M. J. (2016).  
 345 Oceanic eddy detection and lifetime forecast using machine learning methods.  
 346 *Geophysical Research Letters*, 43(23). doi: 10.1002/2016gl071269
- 347 Beron-Vera, F. J., Wang, Y., Olascoaga, M. J., Goni, G. J., & Haller, G. (2013). Ob-  
 348 jective Detection of Oceanic Eddies and the Agulhas Leakage. *Journal of Physical*  
 349 *Oceanography*, 43(7), 1426–1438. doi: 10.1175/JPO-D-12-0171.1
- 350 Bouali, M., Sato, O. T., & Polito, P. S. (2017). Temporal trends in sea surface tem-  
 351 perature gradients in the South Atlantic Ocean. *Remote Sensing of Environment*,  
 352 194, 100–114. doi: 10.1016/j.rse.2017.03.008
- 353 Callies, J., Flierl, G., Ferrari, R., & Fox-Kemper, B. (2015). The role of mixed-layer  
 354 instabilities in submesoscale turbulence. *Journal of Fluid Mechanics*, 788, 5–41.  
 355 doi: 10.1017/jfm.2015.700
- 356 Cane, M. A., Clement, A. C., Kaplan, A., Kushnir, Y., Pozdnyakov, D., Seager, R.,  
 357 ... Murtugudde, R. (1997). Twentieth-Century Sea Surface Temperature Trends.  
 358 *Science*, 275(5302), 957–960. doi: 10.1126/science.275.5302.957
- 359 Chelton, D. B., Gaube, P., Schlax, M. G., Early, J. J., & Samelson, R. M. (2011).  
 360 The influence of nonlinear mesoscale eddies on near-surface oceanic chlorophyll.  
 361 *Science*, 334(6054), 328-32. doi: 10.1126/science.1208897
- 362 Chelton, D. B., & Schlax, M. G. (2013). *Mesoscale eddies in altimeter observations*  
 363 *of ssh*.
- 364 Chelton, D. B., Schlax, M. G., Samelson, R. M., & de Szoeke, R. A. (2007). Global  
 365 observations of large oceanic eddies. *Geophysical Research Letters*, 34(15),  
 366 L15606. doi: 10.1029/2007GL030812
- 367 CMEMS. (2017). The Ssalto/Duacs altimeter products were produced and dis-  
 368 tributed by the Copernicus Marine and Environment Monitoring Service. *Aviso*  
 369 *Dataset*. Retrieved from <https://www.aviso.altimetry.fr/>
- 370 Cui, W., Wang, W., Zhang, J., & Yang, J. (2020). Identification and census statis-  
 371 tics of multicore eddies based on sea surface height data in global oceans. *Acta*

- 372        *Oceanologica Sinica*, 39(1), 41–51. doi: 10.1007/s13131-019-1519-y
- 373        Faghmous, J. H., Frenger, I., Yao, Y., Warmka, R., Lindell, A., & Kumar, V. (2015,  
374        6). A daily global mesoscale ocean eddy dataset from satellite altimetry. *Scientific  
375        Data*, 2, 150028 EP -. doi: 10.1038/sdata.2015.28
- 376        Ferrari, R., & Wunsch, C. (2009). Ocean Circulation Kinetic Energy: Reservoirs,  
377        Sources, and Sinks. *Annual Review of Fluid Mechanics*, 41(1), 253–282. doi: 10  
378        .1146/annurev.fluid.40.111406.102139
- 379        Frenger, I., Gruber, N., Knutti, R., & Münnich, M. (2013). Imprint of Southern  
380        Ocean eddies on winds, clouds and rainfall. *Nature Geoscience*, 6(8), 608 EP -.  
381        doi: 10.1038/ngeo1863
- 382        Frenger, I., Münnich, M., Gruber, N., & Knutti, R. (2015). Southern Ocean eddy  
383        phenomenology. *Journal of Geophysical Research: Oceans*, 120(11), 7413-7449.  
384        doi: 10.1002/2015JC011047
- 385        Fu, L., Chelton, D., Le Traon, P., & Oceanography, M. R. (2010). Eddy dynamics  
386        from satellite altimetry. *Oceanography*, 23(4), 14-25. doi: 10.2307/24860859
- 387        Gill, A., Green, J., & Simmons, A. (1974). Energy partition in the large-scale ocean  
388        circulation and the production of mid-ocean eddies. *Deep Sea Res Oceanogr Abstr*,  
389        21(7), 499-528. doi: 10.1016/0011-7471(74)90010-2
- 390        Hogg, A. M., & Blundell, J. R. (2006). Interdecadal variability of the southern  
391        ocean. *Journal of Physical Oceanography*, 36(8), 1626-1645. doi: 10.1175/  
392        JPO2934.1
- 393        Hogg, A. M., Meredith, M. P., Chambers, D. P., Abrahamsen, E. P., Hughes,  
394        C. W., & Morrison, A. K. (2015). Recent trends in the Southern Ocean  
395        eddy field. *Journal of Geophysical Research: Oceans*, 120(1), 257-267. doi:  
396        10.1002/2014JC010470
- 397        Hu, S., Sprintall, J., Guan, C., McPhaden, M. J., Wang, F., Hu, D., & Cai,  
398        W. (2020, 2). Deep-reaching acceleration of global mean ocean circula-  
399        tion over the past two decades. *Science Advances*, 6(6), eaax7727. doi:  
400        10.1126/sciadv.aax7727
- 401        Kang, D., & Curchitser, E. N. (2017). On the Evaluation of Seasonal Variability of  
402        the Ocean Kinetic Energy. *Geophysical Research Letters*, 47, 1675-1583. doi: 10  
403        .1175/JPO-D-17-0063.1
- 404        Li, G., Cheng, L., Zhu, J., Trenberth, K. E., Mann, M. E., & Abraham, J. P. (2020).

- 405 Increasing ocean stratification over the past half-century. *Nature Climate Change*,  
406 1–8. doi: 10.1038/s41558-020-00918-2
- 407 Martínez-Moreno, J., Hogg, A. M., England, M., Constantinou, N. C., Kiss, A. E.,  
408 & Morrison, A. K. (2021). Global changes in oceanic mesoscale currents over the  
409 satellite altimetry record. *Journal of Advances in Modeling Earth Systems*, 0(ja).  
410 doi: 10.1029/2019MS001769
- 411 Martínez-Moreno, J., Hogg, A. M., Kiss, A. E., Constantinou, N. C., & Mor-  
412 rison, A. K. (2019). Kinetic energy of eddy-like features from sea surface  
413 altimetry. *Journal of Advances in Modeling Earth Systems*, 0(ja). doi:  
414 10.1029/2019MS001769
- 415 Patel, R. S., Llort, J., Strutton, P. G., Phillips, H. E., Moreau, S., Pardo, P. C.,  
416 & Lenton, A. (2020). The Biogeochemical Structure of Southern Ocean  
417 Mesoscale Eddies. *Journal of Geophysical Research: Oceans*, 125(8). doi:  
418 10.1029/2020jc016115
- 419 Pilo, G. S., Mata, M. M., & Azevedo, J. L. L. (2015). Eddy surface properties and  
420 propagation at Southern Hemisphere western boundary current systems. *Ocean  
421 Science*, 11(4), 629–641. doi: 10.5194/os-11-629-2015
- 422 Qiu, B. (1999). Seasonal Eddy Field Modulation of the North Pacific Subtropical  
423 Countercurrent: TOPEX/Poseidon Observations and Theory. *Journal of Physical  
424 Oceanography*, 29(10), 2471–2486. doi: 10.1175/1520-0485(1999)029<2471:sefmot>2  
425 .0.co;2
- 426 Qiu, B., & Chen, S. (2004). Seasonal Modulations in the Eddy Field of the South  
427 Pacific Ocean. *Journal of Physical Oceanography*, 34(7), 1515–1527. doi: 10.1175/  
428 1520-0485(2004)034<1515:smitef>2.0.co;2
- 429 Qiu, B., Chen, S., Klein, P., Sasaki, H., & Sasai, Y. (2014). Seasonal Mesoscale  
430 and Submesoscale Eddy Variability along the North Pacific Subtropical Coun-  
431 tercurrent. *Journal of Physical Oceanography*, 44(12), 3079–3098. doi:  
432 10.1175/jpo-d-14-0071.1
- 433 Ruela, R., Sousa, M. C., deCastro, M., & Dias, J. M. (2020). Global and regional  
434 evolution of sea surface temperature under climate change. *Global and Planetary  
435 Change*, 190, 103190. doi: 10.1016/j.gloplacha.2020.103190
- 436 Sasaki, H., Klein, P., Qiu, B., & Sasai, Y. (2014). Impact of oceanic-scale inter-  
437 actions on the seasonal modulation of ocean dynamics by the atmosphere. *Nature*

- 438                    *Communications*, 5(1), 5636. doi: 10.1038/ncomms6636
- 439                    Schubert, R., Schwarzkopf, F. U., Baschek, B., & Biastoch, A. (2019). Submesoscale  
440                    Impacts on Mesoscale Agulhas Dynamics. *Journal of Advances in Modeling Earth  
441                    Systems*, 11(8), 2745–2767. doi: 10.1029/2019ms001724
- 442                    Siegel, D., Peterson, P., DJ, M., Maritorena, S., & Nelson, N. (2011). Bio-optical  
443                    footprints created by mesoscale eddies in the Sargasso Sea. *Geophysical Research  
444                    Letters*, 38(13), n/a-n/a. doi: 10.1029/2011GL047660
- 445                    Tsujino, H., Urakawa, S., Nakano, H., Small, J. R., Kim, W. M., Yeager, S. G.,  
446                    ... Yamazaki, D. (2018). JRA-55 based surface dataset for driving ocean -  
447                    sea-ice models (JRA55-do). *Ocean Model*, 130, 79 - 139. doi: 10.1016/  
448                    j.ocemod.2018.07.002
- 449                    Uchida, T., Abernathey, R., & Smith, S. (2017). Seasonality of eddy kinetic energy  
450                    in an eddy permitting global climate model. *Ocean Modelling*, 118, 41-58. doi: 10  
451                    .1016/j.ocemod.2017.08.006
- 452                    Wunsch, C. (2020). Is The Ocean Speeding Up? Ocean Surface Energy Trends.  
453                    *Journal of Physical Oceanography*, 50(11), 1–45. doi: 10.1175/jpo-d-20-0082.1
- 454                    Wunsch, C., & Ferrari, R. (2004). VERTICAL MIXING, ENERGY, AND THE  
455                    GENERAL CIRCULATION OF THE OCEANS. *Annual Review of Fluid Me-  
456                    chanics*, 36(1), 281–314. doi: 10.1146/annurev.fluid.36.050802.122121
- 457                    Wyrtki, K., Magaard, L., & Hager, J. (1976). Eddy energy in the oceans. *Journal of  
458                    Geophysical Research*, 81(15), 2641-2646. doi: 10.1029/JC081i015p02641